Efficient Photocatalytic Degradation of Phenol over $Co_3O_4/BiVO_4$ Composite under Visible Light Irradiation

Mingce Long,[†] Weimin Cai,*[,†] Jun Cai,[†] Baoxue Zhou,[†] Xinye Chai,[†] and Yahui Wu[‡]

School of Environment Science and Engineering, Shanghai Jiao Tong University, 800 Dong Chuan Road, Shanghai 200240, China, and Department of Environmental Science and Engineering, School of Civil and Environmental Engineering, Harbin Institute of Technology, Harbin 150090, China

Received: June 3, 2006; In Final Form: July 31, 2006

$Co_3O_4/BiVO_4$ composite photocatalyst with a p−n heterojunction semiconductor structure has been synthesized by the impregnation method. The physical and photophysical properties of the composite photocatalyst have been characterized by X-ray diffraction (XRD), X-ray photoelectron spectroscopy (XPS), transimission electron microscopy (TEM), BET surface area, and UV−visible diffuse reflectance spectra. Co is present as p-type Co_3O_4 and disperses on the surface of n-type $BiVO_4$ to constitute a heterojunction composite. The photocatalyst exhibits enhanced photocatalytic activity for phenol degradation under visible light irradiation. The highest efficiency is observed when calcined at 300 °C with 0.8 wt % cobalt content. On the basis of the calculated energy band positions and PL spectra, the mechanism of enhanced photocatalytic activity has been discussed.

1. Introduction

As visible light accounts for the largest proportion of the solar spectrum, great interests in photocatalysis have been focused on photocatalytic splitting of water or degradation of organic pollutants under visible light irradiation. This is promising for energy and environmental issues.[1−5] There are two strategies to develop the visible-light-driven photocatalysts: modification of TiO_2[6−8] and exploitation of novel semiconductor materials.[9,10] Recently, many investigations have been undertaken on the latter strategy. A great number of novel undoped single-phase mixed oxide semiconductor photocatalysts have been developed, such as $BiVO_4$,[11−13] $CaBi_2O_4$,[10] $PbBi_2Nb_2O_9$,[14] and so on. They all show a certain absorption ability in the visible light range. One characteristic of these photocatalysts is their micro or submicro dimension. The larger sizes as compared to TiO_2 nanoparticles lead to higher density, so they show good precipitation performance and can easily be recovered in water purification. Yet they have some disadvantages such as small specific surface areas, long migration distances for excitated electron−hole pairs, and increasing energy-wasteful recombinations; all of these were expected to lower photocatalytic activities. It is reported that loading a small amount of noble metals or metal oxides, in particular, Pt, Ag, NiO, and RuO_2,[15−17] greatly improves the activity of these photocatalysts. However, some loading species can improve the photocatalytic performance, but others may debase it.[15,16] It is determined by the energy band structures, morphologies, and photoelectrochemical characteristics of the loading species and photocatalysts. So designing more efficient and more easily separable visible-light-driven composite photocatalytic materials, which can meet the requirement of practical environmental application, is the goal of the researchers.

$BiVO_4$ has been used as a pigment for many years. Recently, it has been found that $BiVO_4$ with a monoclinic scheelite structure shows photocatalytic activity for water splitting[11−13] and organic pollutants photodegradation under visible light irradiation.[5] Several methods have been reported for the synthesis of $BiVO_4$, such as solid-state reaction,[11] solution precipitation processes,[12,18] metalorganic decomposition,[19] surfactant-assisted hydrothermal treatment,[20,21] and sonochemical method.[22] Yet the activity of pure $BiVO_4$ is low due to its poor adsorptive performance and difficult migration of electron−hole pairs. Kohtani et al. have reported that the Ag-loaded $BiVO_4$ showed improved activities in photooxidation of polycyclic aromatic hydrocarbons and 4-*n*-alkylphenols under visible light irradiation.[3,4] Yet the photooxidation efficiency of phenol by Ag−$BiVO_4$ is still low, for the adsorption ability of phenol on $BiVO_4$ or Ag−$BiVO_4$ is negligible. Cobalt oxides such as CoO or Co_3O_4 are p-type semiconductors with interesting electronic and magnetic properties. They have found application as efficient catalysts,[23] high-temperature solar selective absorbers,[24] and pigments for glasses and ceramics[25] and have been regarded as the most versatile oxides materials among the transition metal oxides.[25] Yet little attention to cobalt oxides has been taken in the domain of photocatalysis. Recently, it has been reported that the CoO_x/TiO_2[26,27] showed enhanced activity in water splitting and wet oxidation of trichloroethylene,[28] but the mechanism has not been clarified.

Herein, we demonstrated the synthesis, characterization, and photocatalytic properties of $CoO_x/BiVO_4$ composite under visible light irradiation, and we discussed the mechanism of enhanced photocatalytic activity of this composite.

2. Experimental Section

Sample Preparation. All chemicals were reagent grade and used without further purification. $BiVO_4$ powders were synthesized in aqueous medium as reported by Kohtani et al.[4,18] The composite particles were prepared by the impregnation method from an aqueous solution of $Co(NO_3)_2$. The impregnation loading was carried out by the following typical procedure: $BiVO_4$ powder (1.0 g) was added to 1−4 mL of distilled water containing an appropriate amount of $Co(NO_3)_2$ in a ceramic dish. The suspension was stirred using a glass rod during evaporation

* Corresponding author. E-mail: wmcai@sjtu.edu.cn.
[†] Shanghai Jiao Tong University.
[‡] Harbin Institute of Technology.

10.1021/jp063441z CCC: $33.50
Published on Web 09/16/2006

of water under the irradiation of an infrared light. The resulting powder was collected and calcined in air under different temperatures for 2 h. The content of loading species was calculated according to the mass percentage of Co. Co_3O_4 was prepared by calcining the $Co(NO_3)_2$ at 300 °C in the air, and its crystal form has been confirmed by XRD.

Characterization. The crystal structures of photocatalyst powders were characterized by powder X-ray diffraction (XRD, Bruker-AXS D8 Advance) with Cu irradiation. A diffuse reflectance UV−vis spectrophotometer (DRS, Varian Cary 500 Scan) was used to obtain the absorption spectra of samples. The binding energies of Bi, V, O, and Co were measured at room temperature using an X-ray photoelectron spectroscope (XPS, VG Scientific Micro Lab 310F). The peak positions of each element were corrected by using C_{1s} (284.6 eV). The micrograph of the particles was observed using a transmission electron microscope (TEM, JEM-2010 JEOL). The Brunauer−Emmett−Teller (BET) surface area of the samples was determined using a Micromeritrics ASAP 2010 nitrogen adsorption apparatus. The photoluminescence (PL) spectra of photocatalysts were detected with a Jobin Yvon LabRAM HR 800 UV micro-Raman spectrometer using a 325 nm line from an He−Cd laser.

Photocatalytic Reaction. The photocatalytic activity of the samples was evaluated by phenol degradation, because phenol is a typical recalcitrant contaminant without sensitizing as a dye. A 1000-W Xe lamp was used as the light source, and visible light activated photocatalytic activity was tested with any irradiation below 400 nm removed by using a cutoff filter. The temperature of the phenol solution stirred by a magnetic stirrer in an open reactor was about 298 K. Samples were taken at regular time intervals and separated by filtration under reduced pressure. The concentration of phenol was monitored by modified colorimetry with a UNICO UV-2102 spectrometer.[7] The initial and final total organic carbon (TOC) content was determined by a Germany Multi-N/C2000 TOC analyzer to evaluate the photomineralization degree.

3. Results and Discussion

Characterization of Photocatalysts. It has been reported that $BiVO_4$ has three main crystal forms:[12] tetragonal zircon structure, monoclinic scheelite structure, and tetragonal scheelite structure. The phase transition can take place under different temperatures or by crushing the powder at room temperature. Yet only the monoclinic scheelite structure $BiVO_4$ shows good photocatalytic performance under visible light irradiation. So keeping the crystal forms invariant after calcination is necessary. Figure 1 shows the XRD patterns of the prepared pure and CoO_x/$BiVO_4$ composite under various calcination temperatures. Characteristic peaks at 15.2°, 18.7°, 28.6°, 30.5°, and so on were observed for all four diffraction patterns, which are identical to the standard cards (JCPDS 14-0688). This indicates that all samples are monoclinic scheelite structure, and calcination below 400 °C cannot influence the crystal forms of $BiVO_4$. Yet when the sample was calcined at 400 °C, the diffraction pattern showed weak signals at 36.7° (*), which is assigned to the Co_3O_4 (JCPDS 78-1969) on the surface of $BiVO_4$ powder. This indicates the crystallinity of CoO_x species increased at the higher temperature.

To identify the chemical state of Co atoms in the CoO_x/$BiVO_4$ composite particles, the X-ray photoelectron spectroscopy (XPS) of the 0.8% CoO_x/$BiVO_4$ calcined at 300 °C was measured. The Bi_{4f} orbital showed splitting peaks at 159.0 and 164.5 eV (Figure 2a), and the V_{2p} orbital showed peaks at 516.9 and 523.9 eV (Figure 2b). The asymmetric XPS of O_{1s} (Figure 2c)

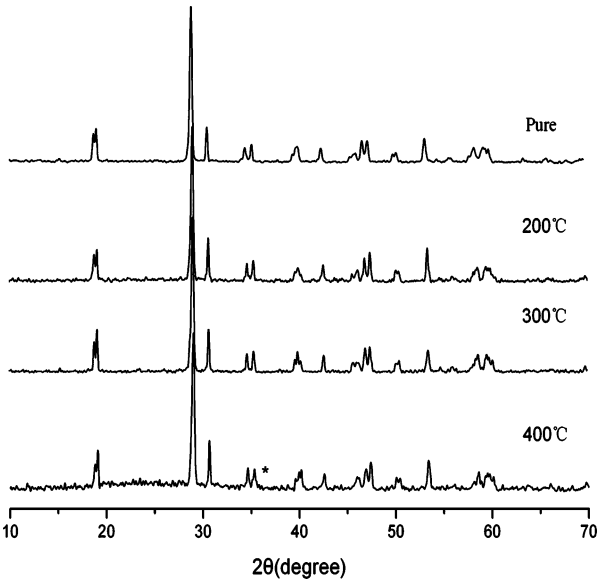

Figure 1. XRD patterns of pure $BiVO_4$ and CoO_x/$BiVO_4$ composite photocatalysts under various calcination temperatures with 0.8 wt % Co content.

indicated that different oxygen species were present in the near surface region. They are the lattice oxygen (530.3 eV) in crystalline $BiVO_4$ or CoO_x and the chemisorbed OH^- (531.6 eV) on the surface.[13] Wu et al. analyzed the Co species by XPS in the CoO_x-modified TiO_2, and they thought Co was presented as CoO at high content but complex CoO_x at low content.[26] Yet we found the Co $2p_{3/2}$ and Co $2p_{1/2}$ main peaks are located at 780.9 and 796.9 eV (Figure 2d). These peaks are very close to those of Co_3O_4, whose corresponding peaks are reported at 780.8 and 796.8 eV.[29] Zhou et al. prepared Co_3O_4 nanoparticles by calcining samples at 300 °C in a flow of air.[30] We also obtained pure Co_3O_4 by calcining $Co(NO_3)_2$ at 300 °C. So it can be deduced that the Co is present as Co_3O_4 in this sample.

The color of the CoO_x/$BiVO_4$ composite powders is dark green and becomes darker and darker by enhancing the Co content and increasing the calcination temperature. Figure 3a shows the diffuse reflection spectra (DRS) of pure and Co_3O_4/$BiVO_4$ composite. The band gap absorption edge of pure $BiVO_4$ is determined to be 545 nm, corresponding to the band gap energy 2.28 eV, and it is the directly allowed optical transition (Figure 3b). It is slightly smaller than the reported values,[3,11,12] which can be attributed to large particle sizes and surface defects. After Co_3O_4 was loaded, the ability of light absorption is enhanced greatly. This should be attributed to the small band gap of Co_3O_4, which is a p-type semiconductor with direct transition at 1.45 and 2.07 eV,[29] corresponding respectively to edges of $O^{2-} \rightarrow Co^{3+}$ excitation and $O^{2-} \rightarrow Co^{2+}$ charge transfer. The latter is the basic optical band gap energy for interband transitions.[31,32] There are two absorption bands in the Co_3O_4/$BiVO_4$ composite that can be attributed to the two transitions of Co_3O_4, but with a slight blue shift because of the presence of $BiVO_4$. Co_3O_4 has absorption in nearly all of the visible light range. This fact induces an extension of the light absorption spectrum of the composite semiconductor even at low cobalt contents.

Figure 4 shows the transmission electron microscopy (TEM) image of a typical Co_3O_4/$BiVO_4$ composite particle. The image in Figure 4a demonstrates that the $BiVO_4$ particles prepared under our procedure are micro particles with several micrometer sizes, and this large dimension can induce a good precipitation performance. It clearly exhibits that small hetero particles

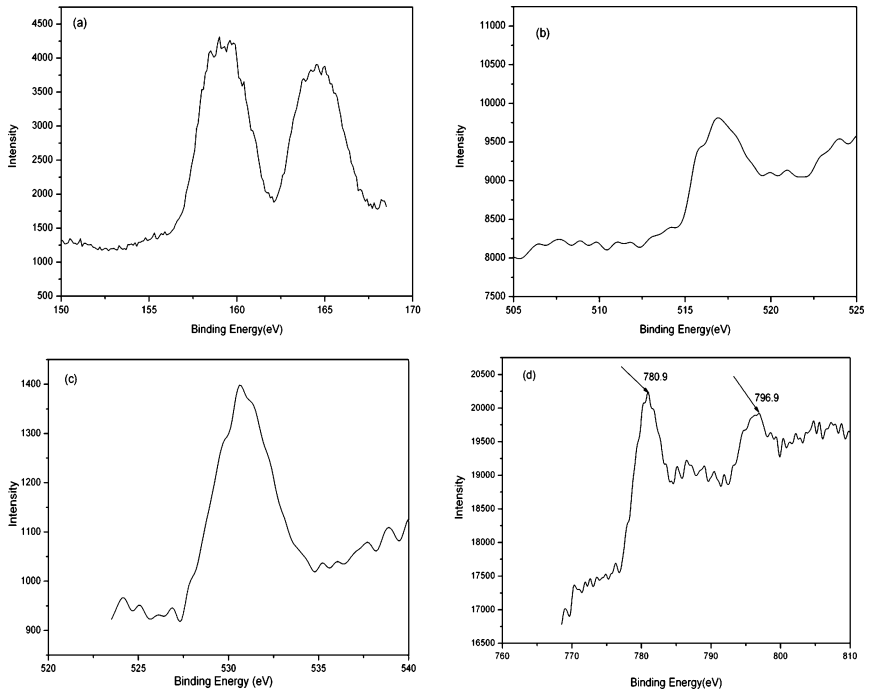

Figure 2. XPS spectrum analysis of Bi_{4f} (a), V_{2p} (b), O_{1s} (c), and Co_{2p} (d) for 0.8 wt % $CoO_x/BiVO_4$ composite calcined at 300 °C.

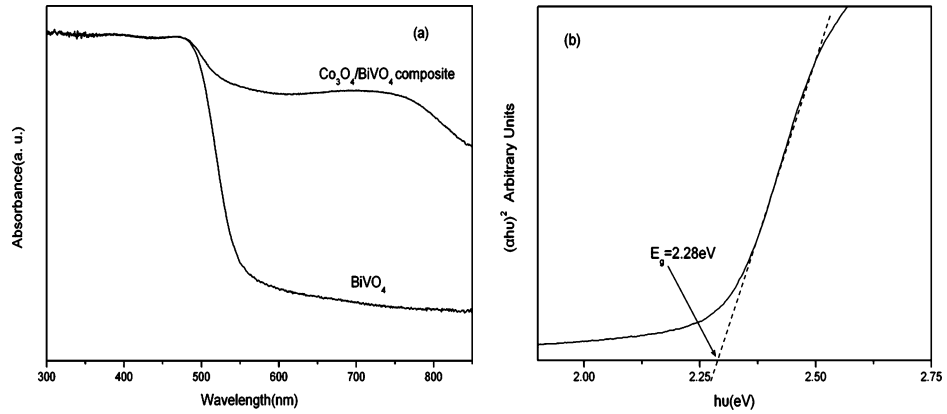

Figure 3. UV−vis diffuse absorption spectra of photocatalysts (a) and estimated band gap of $BiVO_4$ by Kubelka−Munk function (b).

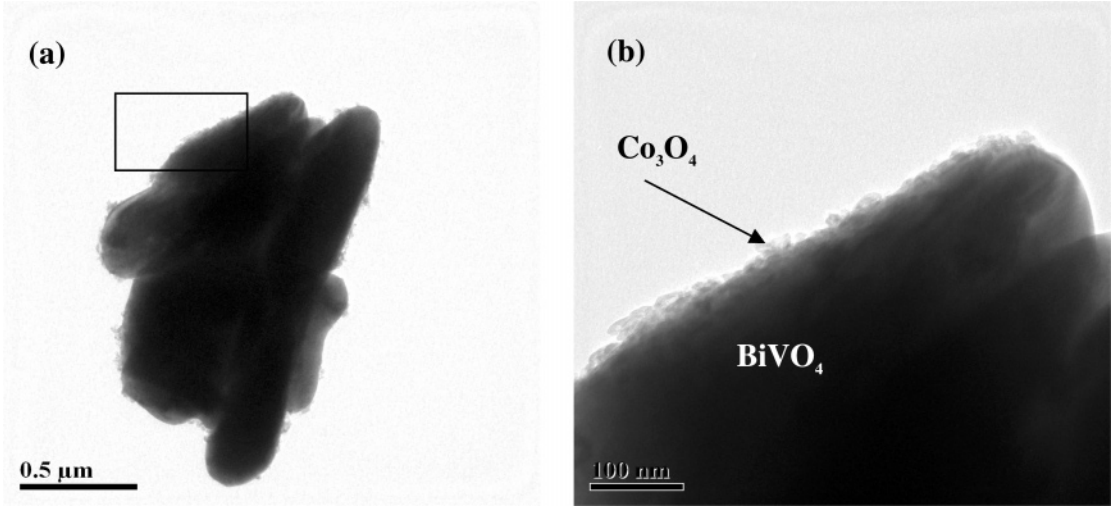

Figure 4. TEM image of the $Co_3O_4/BiVO_4$ composite (a) and the magnified views of the composite heterojunction structure (b).

disperse over the edge of large $BiVO_4$ particles, and the shape of $BiVO_4$ particles is irregular. The magnified views in Figure 4b show that the Co_3O_4 powder is comprised of nanoparticles with sizes of 20−50 nm, deposited over the surface of $BiVO_4$, and they constitute a kind of composite heterojunction structure. The phase identification was also confirmed by elemental analysis with in situ energy-dispersive X-ray microanalysis carried out during the microscopic study.

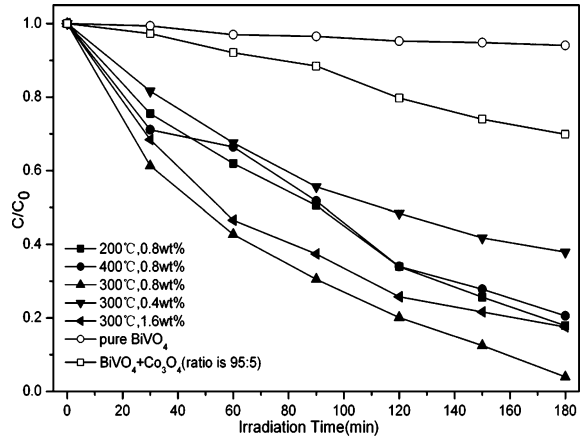

Figure 5. The decrease of phenol by different photocatalysts as a function of visible light irradiation time. The used photocatalysts are $BiVO_4$, $BiVO_4$ and Co_3O_4 mixture, and $CoO_x/BiVO_4$ composite calcined at different temperatures for 2 h with different Co contents (photocatalysts loading, 3 g/L; initial phenol concentration, about 18 mg/L; without pH modulation).

The BET surface area of $Co_3O_4/BiVO_4$ composite is 1.38 $m^2\ g^{-1}$, which is larger than that of $BiVO_4$ powder (0.74 $m^2\ g^{-1}$). The enlarged BET is attributed to introducing the nanoparticles Co_3O_4 on the surface of $BiVO_4$. Yet their BET values are nearly of the same magnitude, both of which are still very low as compared to that of nanoparticle TiO_2.

Photocatalytic Activity of the Prepared Samples. Photocatalytic activity of $CoO_x/BiVO_4$ composites has been evaluated by degradation of phenol under visible light irradiation. Phenol is hardly adsorbed on catalysts such as TiO_2 or $BiVO_4$[3] from its aqueous solution, so its photodegradation is always more difficult than those adsorbable pollutants.

Figure 5 shows the effect of Co content and calcination temperature on the photodegradation activity of phenol under visible light irradiation. A blank experiment in the absence of irradiation but with the catalysts demonstrated that no significant change in the phenol concentration was found. The decrease of phenol concentration in the presence of pure $BiVO_4$ under visible light is very small, only about 6% in 180 min. The performance can be improved when introducing Co_3O_4; the reduction of phenol is 30.1% in 180 min in the presence of a 95% $BiVO_4$ and 5% Co_3O_4 mixture. Yet after CoO_x was loaded, the composite photocatalysts showed significantly enhanced activity.

Calcination temperature and Co content are important factors for the morphology of loaded species,[16] which is pivotal for producing $CoO_x/BiVO_4$ composite with high activity. After being impregnated, the $Co(NO_3)_2$ particles distribute on the surface of $BiVO_4$. By calcination at various temperatures, the $Co(NO_3)_2$ decomposed into cobalt oxides species, and its crystallinity was improved by increasing temperature. Highly crystallized structure always favors migration of electron−hole pairs as compared to the amorphous structure, so as to high photocatalytic activity. Yet at higher temperatures, the CoO_x agglomerates into large bulk low activity species,[16] and the activity would be debased. Suitable content of loaded Co also leads to fine particle dispersion on the $BiVO_4$ surface with high activity. Yet at higher Co content, the nanoclusters of CoO_x species would form overlapping agglomerates and smother the surface of $BiVO_4$, therefore lowering the activity for phenol photodegradation. So there are optimum calcination temperatures and cobalt contents for high dispersion morphology of nanoclusters CoO_x with high activity. In our result (Figure 5), the composite sample calcined at 300 °C with 0.8 wt % CoO_x exhibits the best activity, with the phenol concentration reduced as much as 96.0% in 180 min. The TOC of this sample decreased from 17.80 to 2.52 mg/L. This confirmed that phenol has been not only degraded but also mineralized efficiently upon the $CoO_x/BiVO_4$ composite. This composite photocatalyst shows photocatalytic power superior to that of our recent report of iodine-doped TiO_2.[7] It also exhibits good precipitation performance, which deposits into the bottom of the reactor in 30 min. The easy separation property is an important prerequisite for practical environmental purification application.[33] Because of its highest activity when it is calcined at 300 °C with 0.8 wt % Co content, the rest of the experiments were carried out using this material, which was assigned as $Co_3O_4/BiVO_4$ composite.

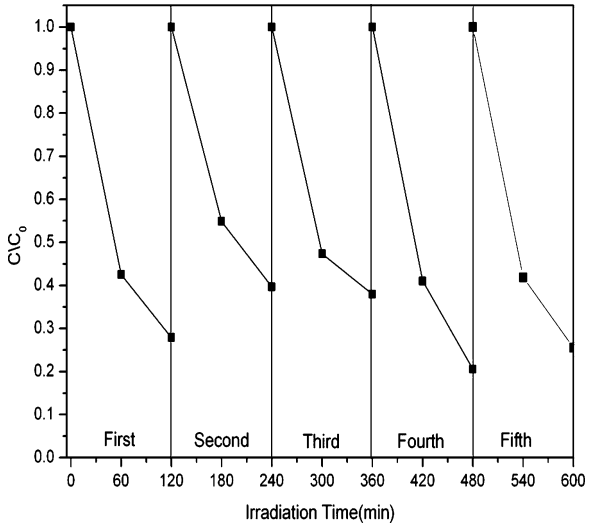

Figure 6. Cycling runs in photocatalytic degradation of phenol in the presence of $Co_3O_4/BiVO_4$ composite under visible light irradiation (photocatalysts loading, 3 g/L; initial phenol concentration, about 18 mg/L; without pH modulation).

The stability of the novel composite was evaluated by recycled experiments. During the first three runs, the photocatalysts were not transferred out. Yet after every 2 h of photodegradation, the concentrated phenol solution was injected and the separated photocatalysts were washed back with distilled water into the reactor, so as to keep the initial concentration of phenol and photocatalysts constant. In the last two recycled tests, we separated the photocatalysts by centrifuging, washing with distilled water, and drying. The decrease of phenol in every run is shown in Figure 6. After the first three runs, the activity of composite photocatalysts debased slightly because there were some intermediates adsorbed on the surface.[34] After being separated, dried, and then recycled, the photocatalysts exhibit even higher activity than in the first run. So this indicates that the composite photocatalysts are stable in photocatalysis. It is another prerequisite as compared to doped TiO_2, which always suffers from an instability problem. Cobalt is also cheaper than noble metals such as Ag, Ru, or Pt, so the $Co_3O_4/BiVO_4$ composite photocatalyst is promising for practical application in water purification.

Discussion of Mechanism. The composite photocatalysts have attracted increasing attention for their enhanced performance.[1,35−37] Yet present explanations are still far from clarifying it. In a contrast experiment, $Co_3O_4/BiVO_4$ composite exhibits higher activity than Ag loaded $BiVO_4$ (only 55% phenol reduced in 180 min by Ag loaded $BiVO_4$), and the phenol adsorption on these photocatalysts is very low. So we should continue with a further discussion on the mechanism in the photocatalysis.

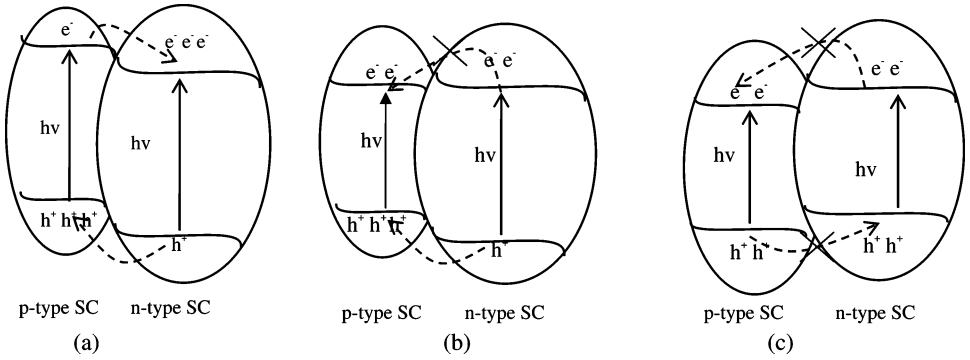

Figure 7. Proposed principle of charge separation for p−n heterojunction semiconductor photocatalysts under irradiation.

Co_3O_4 is a p-type semiconductor (SC), which always exhibits good stability under illumination,[38] and $BiVO_4$ is determined as an n-type material.[39] So at the interfaces of Co_3O_4 loaded $BiVO_4$ composite, a p−n heterojunction would be formed. Generally there are three kinds of band edge positions between two p−n heterojunction interfaces. They are depicted in Figure 7.

At the thermodynamic equilibrium of a p−n heterojunction SC, there is an internal field with direction from n-type SC to p-type SC. Figure 7a is the most favorable one for photocatalysis. According to the band edge position, the excited electrons on the conduction band of the p-type SC transfer to that of the n-type SC, and simultaneous holes on the valence band of n-type SC can be transferred to that of p-type SC under the potential of the band energy difference. The migration of photogenerated carriers can be promoted by the internal field, so less of a barrier exists. Therefore, the recombination of electron−hole pairs can be reduced, and the photocatalytic reaction can be enhanced greatly. The second case (Figure 7b) is also favorable for photocatalysis. The holes can transfer from n-type SC to p-type easily, but the electrons cannot transfer from n-type SC to p-type. If electrons transferred to p-type SC, the photocatalytic activity would decrease because of recombination.[40] Although the transfer of electrons is feasible for the potential between the two conduction bands, it is blocked because of the internal fields. So the minor carrier in n-type SC, which is the control factor of recombination in this type SC, can transfer out. The net effect in this case also reduces the energy wasteful recombination of charge carriers and facilitates the photodegradation of organic pollutant. The third case (Figure 7c) is invalid for the separation of photogenerated electrons and holes because the internal fields block migration.

The above analysis shows that the migration direction of the photogenerated charge carrier depends on the band edge positions of the two semiconductors. There are three methods to determine the band edge positions: experiments based on photoelectrochemical techniques, calculation according to the first principle, and predicting theoretically from the absolute (or Mulliken) electronegativity.[41−43] The first one is not always easy to handle, and the second one cannot obtain the absolute energy of band edges with respect to vacuum and always has large discrepancies between calculated and measured values. The third one is a simple approach with reasonable results for many oxides photocatalysts.[42,43] The conduction band edge of a semiconductor at the point of zero charge (pH_{zpc}) can be predicted by eq 1:

$$E_{CB}{}^{0} = X - E^{c} - {}^{1}/_{2}\,E_{g} \qquad (1)$$

where X is the absolute electronegativity of the semiconductor, expressed as the geometric mean of the absolute electronegativity of the constituent atoms, which is defined as the arithmetic mean of the atomic electron affinity and the first ionization energy; E^c is the energy of free electrons on the hydrogen scale (~4.5 eV); and E_g is the band gap of the semiconductor. The predicted band edge positions of Co_3O_4 and $BiVO_4$ by the above equation are shown in Table 1. In fact, these values are slightly more anodic than the measured value, but this does not affect the comparison of their relative positions. According to the estimated E_g values of $BiVO_4$ by our result, the conduction band position of $BiVO_4$ is more anodic than Co_3O_4, and the schematic energy band model of the composite can be depicted as Figure 7a. Yet when estimated from the reference value, the conduction band positions are reversed, and the model can be depicted as Figure 7b. Both cases are favorable for separation of electron−hole pairs. So this $Co_3O_4/BiVO_4$ composite exhibits enhanced performance as compared to pure $BiVO_4$.

TABLE 1: Absolute Electronegativity, Estimated Band Gap, Energy Levels of Calculated Conduction Band Edge, and Valence Band at the Point of Zero Charge for Co_3O_4 and $BiVO_4$

semiconductor oxides	absolute electronegativity (X)	estimated energy band gap E_g (eV)	calculated conduction band edge (eV)	calculated valence band edge (eV)
Co_3O_4	5.903	2.07	0.37	2.44
$BiVO_4$	6.035	2.28[a]/2.4[b]	0.39/0.33	2.67/2.73

[a] Estimated from our result. [b] From references.

To establish the above analysis, we measured the photoluminescence (PL) spectra of the photocatalysts, which are useful to disclose the migration, transfer, and recombination processes of the photogenerated electron−hole pairs in the SC.[44] Kudo et al. did not observe PL of monoclinic $BiVO_4$ at 77 K and considered the recombination as nonradiation.[40] Yet our result is different. Figure 8 shows the PL spectra of $BiVO_4$ and $Co_3O_4/BiVO_4$ composite at 83 and 300 K. Monoclinic $BiVO_4$ has an obvious peak at 600 nm in the PL spectrum, which is very close to that of tetragonal $BiVO_4$.[45] The intensity of the PL decreases significantly at room temperature, but a peak at 600 nm still can be observed. The luminescence corresponds to the recombination of the hole formed in the O_{2p} band and the electron in the V_{3d} band. The PL of $Co_3O_4/BiVO_4$ composite nearly disappears completely. The results clearly show that the recombination of photogenerated charge carrier between O_{2p} and V_{3d} was inhibited greatly in the composite semiconductors. So no photoluminescence can be observed. This result shows good agreement with the analysis by the energy band position of the p−n heterojunction semiconductors, as discussed above.

It can be established that p−n heterojunction composite photocatalysts with proper energy band positions are very promising for photocatalysis with satisfying efficiency. Co_3O_4 is one of the few p-type semiconductors that can easily form

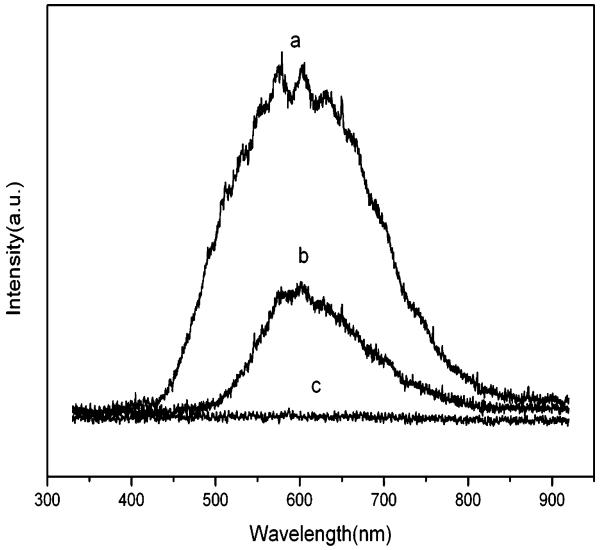

Figure 8. Photoluminescence spectra of $BiVO_4$ at 83 K (a), $BiVO_4$ at 300 K (b), and $Co_3O_4/BiVO_4$ composite at 300 K (c).

p−n heterojunction composites and has potential in photocatalytic functional materials.

4. Conclusion

$Co_3O_4/BiVO_4$ composite photocatalyst has been prepared by impregnation methods. The $BiVO_4$ particles retain monoclinic scheelite structures after being calcined. Co is present as Co_3O_4 and disperses on the surface of $BiVO_4$ to constitute the heterojunction composite. The composite photocatalyst exhibits enhanced photocatalytic activity under visible light irradiation, and the highest efficiency is observed at 0.8 wt % cobalt content and calcined at 300 °C. The mechanism has been discussed by calculated energy band positions and PL spectra. The enhanced activity is attributed to the p−n heterojunction semiconductor structure and the decreasing recombination of photogenerated hole−electron pairs. The composite photocatalyst is promising for water purification application for its good precipitation performance and stability. The activity can be further improved by reducing the dimension of $BiVO_4$ and preparing a nanodimension p−n heterojunction with an ohmic contact.

Acknowledgment. We are thankful for financial support by the Specialized Research Fund for the Doctoral Program of Higher Education (SRFDP, 20050248015) from the Ministry of Education. We gratefully acknowledge the support for transmission electron microscopy (TEM) measurements by Ms. Ruibin Wang and Ms. Xinqiu Guo of the Instrumental Analysis Center of Shanghai Jiao Tong University.

References and Notes

(1) Kim, H. G.; Borse, P. H.; Choi, W.; Lee, J. S. *Angew. Chem., Int. Ed.* **2005**, *44*, 4585.
(2) Liu, H. M.; Nakamura, R.; Nakato, Y. *ChemPhysChem* **2005**, *6*, 2499.
(3) Kohtani, S.; Hiro, J.; Yamamoto, N.; Kudo, A.; Tokumura, K.; Nakagaki, R. *Catal. Commun.* **2005**, *6*, 185.
(4) Kohtani, S.; Tomohiro, M.; Tokumura, K.; Nakagaki, R. *Appl. Catal., B* **2005**, *58*, 265.
(5) Kohtani, S.; Koshiko, M.; Kudo, A.; Tokumura, K.; Ishigaki, Y.; Toriba, A.; Hayakawa, K.; Nakagaki, R. *Appl. Catal., B* **2003**, *46*, 573.
(6) Asahi, R.; Morikawa, T.; Ohwaki, T.; Aoki, K.; Taga, Y. *Science* **2001**, *293*, 269.
(7) Hong, X. T.; Wang, Z. P.; Cai, W. M.; Lu, F.; Zhang, J.; Yang, Y. Z.; Ma, N.; Liu, Y. J. *Chem. Mater.* **2005**, *17*, 1548.
(8) Sakthivel, S.; Kisch, H. *Angew. Chem., Int. Ed.* **2003**, *42*, 4908.
(9) Kudo, A.; Kato, H.; Tsuji, I. *Chem. Lett.* **2004**, *33*, 1534.
(10) Tang, J. W.; Zou, Z. G.; Ye, J. H. *Angew. Chem., Int. Ed.* **2004**, *43*, 4463.
(11) Kudo, A.; Ueda, K.; Kato, H.; Mikami, I. *Catal. Lett.* **1998**, *53*, 229.
(12) Tokunaga, S.; Kato, H.; Kudo, A. *Chem. Mater.* **2001**, *13*, 4624.
(13) Liu, H. M.; Nakamura, R.; Nakato, Y. *J. Electrochem. Soc.* **2005**, *152*, G856.
(14) Kim, H. G.; Hwang, D. W.; Lee, J. S. *J. Am. Chem. Soc.* **2004**, *126*, 8912.
(15) Ishihara, T.; Baik, N. S.; Ono, N.; Nishiguchi, H.; Takita, Y. *J. Photochem. Photobiol., A* **2004**, *167*, 149.
(16) Teramura, K.; Maeda, K.; Saito, T.; Takata, T.; Saito, N.; Inoue, Y.; Domen, K. *J. Phys. Chem. B* **2005**, *109*, 21915.
(17) Tang, J. W.; Zou, Z. G.; Ye, J. H. *J. Phys. Chem. Solids* **2005**, *66*, 349.
(18) Kohtani, S.; Makino, S.; Kudo, A.; Tokumura, K.; Ishigaki, Y.; Matsunaga, T.; Nikaido, O.; Hayakawa, K.; Nakagaki, R. *Chem. Lett.* **2002**, 660.
(19) Sayama, K.; Nomura, A.; Zou, Z. G.; Abe, R.; Abe, Y.; Arakawa, H. *Chem. Commun.* **2003**, 2908.
(20) Zhang, L.; Chen, D. R.; Jiao, X. L. *J. Phys. Chem. B* **2006**, *110*, 2668.
(21) Yu, J. Q.; Kudo, A. *Chem. Lett.* **2005**, *34*, 850.
(22) Zhou, L.; Wang, W. Z.; Liu, S. W.; Zhang, L. S.; Xu, H. L.; Zhu, W. *J. Mol. Catal. A* **2006**, *252*, 120.
(23) Hagelin-Weaver, H. A. E.; Hoflund, G. B.; Minahan, D. M.; Salaita, G. N. *Appl. Surf. Sci.* **2004**, *235*, 420.
(24) Barrera, E.; Gonzalez, I.; Viveros, T. *Sol. Energy Mater. Sol. Cells* **1998**, *51*, 69.
(25) Patil, P. S.; Kadam, L. S.; Lokhande, C. D. *Thin Solid Films* **1996**, *272*, 29.
(26) Wu, Y. Q.; Lu, G. X.; Li, S. B. *Chin. Inorg. Chem.* **2005**, *21*, 309.
(27) Wu, Y. Q.; Lu, G. X.; Li, S. B. *Acta Chim. Sin.* **2005**, *63*, 671.
(28) Kim, M. H. *Korean J. Chem. Eng.* **2005**, *22*, 839.
(29) Gulino, A.; Fragala, I. *Inorg. Chim. Acta* **2005**, *358*, 4466.
(30) Zhou, L. P.; Xu, J.; Li, X. Q.; Wang, F. *Mater. Chem. Phys.* **2006**, *97*, 137.
(31) Cheng, C. S.; Serizawa, M.; Sakata, H.; Hirayama, T. *Mater. Chem. Phys.* **1998**, *53*, 225.
(32) Barreca, D.; Massignan, C.; Daolio, S.; Fabrizio, M.; Piccirillo, C.; Armelao, L.; Tondello, E. *Chem. Mater.* **2001**, *13*, 588.
(33) Hu, J. S.; Ren, L. L.; Guo, Y. G.; Liang, H. P.; Cao, A. M.; Wan, L. J.; Bai, C. L. *Angew. Chem., Int. Ed.* **2005**, *44*, 1269.
(34) Jing, L. Q.; Xin, B. F.; Yuan, F. L.; Wang, B. Q.; Shi, K. Y.; Cai, W. M.; Fu, H. G. *Appl. Catal., A* **2004**, *275*, 49.
(35) Luo, J. H.; Maggard, P. A. *Adv. Mater.* **2006**, *18*, 514.
(36) Maeda, K.; Teramura, K.; Lu, D.; Takata, T.; Saito, N.; Inoue, Y.; Domen, K. *Nature* **2006**, *440*, 295.
(37) Wang, D. F.; Zou, Z. G.; Ye, J. H. *Chem. Mater.* **2005**, *17*, 3255.
(38) Trari, M.; Bouguelia, A.; Bessekhouad, Y. *Sol. Energy Mater. Sol. Cells* **2006**, *90*, 190.
(39) Vinke, I. C.; Diepgrond, J.; Boukamp, B. A.; de Vries, K. J.; Burggraaf, A. J. *Solid State Ionics* **1992**, *57*, 83.
(40) Li, D.; Haneda, H.; Ohashi, N.; Hishita, S.; Yoshikawa, Y. *Catal. Today* **2004**, *93*−*95*, 895.
(41) Kim, Y. I.; Atherton, S. J.; Brigham, E. S.; Mallouk, T. E. *J. Phys. Chem.* **1993**, *97*, 11802.
(42) Butler, M. A.; Ginley, D. S. *J. Electrochem. Soc.* **1978**, *125*, 228.
(43) Xu, Y.; Schoonen, M. A. A. *Am. Mineral.* **2000**, *85*, 543.
(44) Tang, J. W.; Zou, Z. G.; Ye, J. H. *J. Phys. Chem. B* **2003**, *107*, 14265.
(45) Kudo, A.; Omori, K.; Kato, H. *J. Am. Chem. Soc.* **1999**, *121*, 11459.